Position-Controlled Synchronous Reluctance Motor Without Rotational Transducer

Jung-Ik Ha, *Student Member, IEEE,* Seog-Joo Kang, *Member, IEEE,* and Seung-Ki Sul, *Senior Member, IEEE*

***Abstract*— This paper presents a position sensorless control scheme of a synchronous reluctance motor (SynRM) combining a high-frequency current injection method in the low-speed region and the flux estimation method based on the stator voltages in the high-speed region. The rotor has inherent saliency, and its angle can be estimated from d-axis stator current injection and the appropriate signal demodulation in a low-speed region. In the high-speed region, the rotor angle can be estimated by the stator flux from the voltage information. This scheme gives a robust and dynamic estimation of the rotor angle independent of the operating conditions, including speed and load conditions. Experimental results of closed-loop speed and position control with a 3.75-kW axially laminated SynRM are given to verify the proposed scheme.**

***Index Terms*— Current injection method, sensorless control, synchronous reluctance motor.**

I. Introduction

THE synchronous reluctance motor (SynRM) has recently attracted the efforts of a number of researchers and is gaining favor as a possible alternative for ac drives [1]–[3]. Since the converter-fed SynRM does not need a starting cage, an optimized rotor for synchronous performance can be designed. The simple and rugged structure allows high-speed drives to be readily attained, while the copper and iron losses confined in the stator allow the motor to be operated with high electric and magnetic loads with an advantage to the torque/weight ratio. However, a drawback of these drives resides in the need of synchronization with the rotor position. Thus, a rotor position transducer is usually used, resulting in an increase in the cost and a decrease in the reliability of the drive.

Rotor-position-sensing techniques without rotating shaft sensors have been recently addressed [4]–[12]. The current angle detection scheme was developed in [4], however, the detected angle was not used to control an inverter. Another position-sensing scheme [5] provides rotor position information at the zero crossings of the phase current, that is, only six rotor position samples per one electrical cycle of a three-phase motor. The speed control bandwidth would be limited to an unreasonably low value due to this inherent limitation of angle information, in particular, at low speed. Reference [6] proposed torque vector control of a SynRM without a position sensor, and its position-detecting scheme is based on the detection of flux angle by voltage integration. The controllable low speed is limited in this method because the signal-to-noise ratio of voltage is very poor at low speed. A position-detection method using the third harmonic of the stator phase voltage was proposed in [7]. Its results are good, however, it has the drawback of accessing the neutral point of the motor, which is generally difficult. Other approaches [8], [9] to estimate the rotor angle are based on the variation of inductance. These methods can estimate the rotor angle at very low speed and even standstill, but the generated signals are rather noisy because they are based on the differentiating operation. Position-estimation schemes by injecting high-frequency current or voltage were proposed for induction motors in [10]–[13]. The advantages of these methods are independence from loading conditions, robustness to parameter variation, and good and stable low-speed operation. In [12], magnetic saliency in the induction machine was introduced via a modulation of the rotor slot leakage. In these schemes, the bandwidth of the current regulator must be much lower than the injected frequency, because the high-frequency voltage commands can be directly impressed on the fundamental voltage command without the distortion of current by the current regulator.

This paper presents a position sensorless control scheme of a SynRM combining the high-frequency current injection method in the low-speed region and the flux estimation method based on the stator voltages in the high-speed region. The rotor has inherent saliency, and its angle is estimated using the saliency from d-axis stator current injection and the appropriate signal demodulation in the low-speed region. The modulated signal output gives the information of the difference of the real rotor angle and the estimated angle. By adjusting the estimated angle with the modulated signal, continuous position estimation is possible. In a high-speed region, the controllable voltage margin decreases because of the voltage due to the voltage drop of high frequency, and the injected current causes additional losses and noise. Therefore, it is effective for estimating the stator flux from the voltage information in the high-speed region, since there is sufficient voltage magnitude in the region. This scheme gives robust dynamic estimation of

Paper IPCSD 99–48, presented at the 1998 Industry Applications Society Annual Meeting, St. Louis, MO, October 12–16, and approved for publication in the IEEE TRANSACTIONS ON INDUSTRY APPLICATIONS by the Industrial Drives Committee of the IEEE Industry Applications Society. Manuscript released for publication May 5, 1999.

J.-I. Ha and S.-K. Sul are with the School of Electrical Engineering, Seoul National University, Seoul 151-742, Korea (e-mail: haji@eepel.snu.ac.kr; sulsk@plaza.snu.ac.kr).

S.-J. Kang is with the Building Systems Research Laboratory, LG Industrial Systems Company, Ltd., Incheon 402-200, Korea (e-mail: sjkang@lgis.lg.co.kr).

Publisher Item Identifier S 0093-9994(99)07489-7.

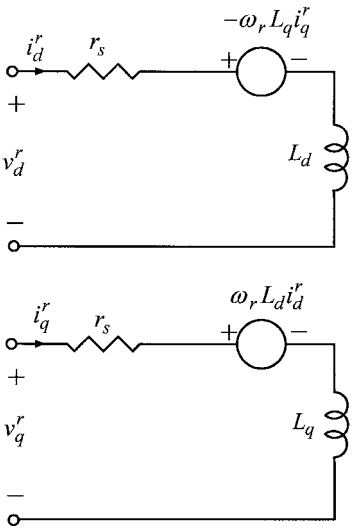

Fig. 1. Equivalent circuit of SynRM.

the rotor angle, independent of the operating speed and load condition.

II. Estimation of Rotor Position

Fig. 1 shows the equivalent circuits of an SynRM in the synchronously rotating rotor reference frame. The voltage equations of the SynRM can be represented as

$$v_d^r = r_s i_d^r + L_d \frac{di_d^r}{dt} - \omega_r L_q i_q^r \tag{1}$$

$$v_q^r = r_s i_q^r + L_q \frac{di_q^r}{dt} + \omega_r L_d i_d^r \tag{2}$$

where

v_d^r, v_q^r	d- and q-axes stator voltages [V];
i_d^r, i_q^r	d- and q-axes rotor currents [A];
r_s	stator resistance [Ω];
L_d	d-axis inductance [H];
L_q	q-axis inductance [H];
ω_r	rotor angular velocity [rad/s].

The generated torque of the SynRM is

$$T_e = \frac{3}{2}\frac{P}{2}(L_d - L_q) i_d^r i_q^r \tag{3}$$

where P is the number of poles.

A. Low-Speed Region—High-Frequency Current Injection

Fig. 2 shows the current vector diagram of a SynRM. D^r and q^r represent the real synchronously rotating rotor reference frame attached to the rotor, and d^c, q^c represent the estimation frame. The angle difference of two frames is denoted as $\Delta\theta_r$, which must be estimated.

At injected high frequency, the voltage equations of a SynRM can be written as follows:

$$\tilde{v}_d^r \approx (r_s + L_d p)\tilde{i}_d^r \tag{4}$$

$$\tilde{v}_p^r \approx (r_s + L_q p)\tilde{i}_q^r \tag{5}$$

where p is the differential operator,

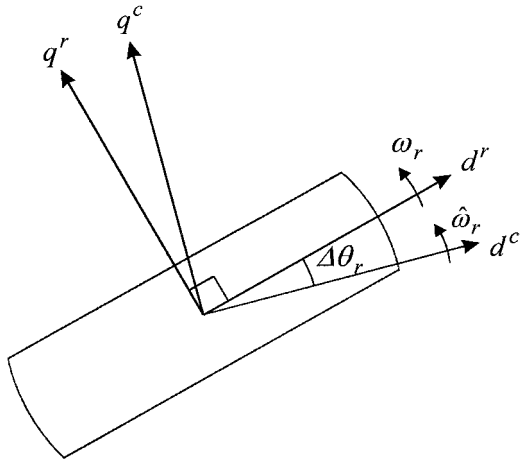

Fig. 2. Current vector diagram.

The superscript "~" denotes the high-frequency component.

To estimate $\Delta\theta_r$, the high-frequency current $\tilde{i}_d^{c^*}$ is injected on the d axis of the estimated frame. It is added to the output current $I_d^{c^*}$ of the speed control loop. Then,

$$i_d^{c^*} = I_d^{c^*} + \tilde{i}_d^{c^*} \tag{6}$$

where $\tilde{i}_d^{c^*} = I_h \cos\omega_h t$, I_h is the magnitude of injected current, andω_h is the angular velocity of injected current. The superscript "*" denotes the reference.

Then, the currents in the rotor reference frame can be written as follows:

$$\tilde{i}_d^r = \tilde{i}_d^c \cos\Delta\theta_r \tag{7}$$

$$\tilde{i}_{qs}^r = -\tilde{i}_d^c \sin\Delta\theta_r. \tag{8}$$

At high frequency, the cross-coupling voltages measured on the estimated rotor reference frame are as follows:

$$\begin{aligned}\tilde{v}_d^c &= \tilde{v}_d^r \sin\Delta\theta_r - \tilde{v}_q^r \sin\theta_r \\ &= r_s\tilde{i}_d^c + (L_d \cos^2\Delta\theta_r + L_q \sin^2\Delta\theta_r)\cdot p\tilde{i}_d^c \\ &\quad - \left\{\frac{1}{2}(L_d - L_q)\sin 2\Delta\theta_r\right\}\tilde{i}_d^c \cdot p\Delta\theta_r.\end{aligned} \tag{9}$$

$$\begin{aligned}\tilde{v}_q^c &= \tilde{v}_d^r \sin\Delta\theta_r + \tilde{v}_q^r \cos\Delta\theta_r \\ &= \left\{\frac{1}{2}(L_d - L_q)\sin 2\Delta\theta_r\right\}\cdot p\tilde{i}_d^c \\ &\quad - (L_d \sin^2\Delta\theta_r + L_q \cos^2\Delta\theta_r)\tilde{i}_d^c \cdot p\Delta\theta_r.\end{aligned} \tag{10}$$

At zero or low speed, if the estimated angle error $\Delta\theta_r$ is small and its variation is slow, the second terms of the above equations can be neglected

$$\tilde{v}_d^c \approx r_s\tilde{i}_d^c + L_d p\tilde{i}_d^c \tag{11}$$

$$\tilde{v}_q^c \approx \{\tfrac{1}{2}(L_d - L_q)\sin 2\Delta\theta_r\}\cdot p\tilde{i}_d^c. \tag{12}$$

A demodulating technique can be utilized to extract the position information from the voltages $\tilde{v}_d^c, \tilde{v}_q^c$. The voltage measured on the quadrature axis of the estimated rotor angle presents the estimated angle error. To avoid the effect of the phasor of high-frequency current, the error can be defined as

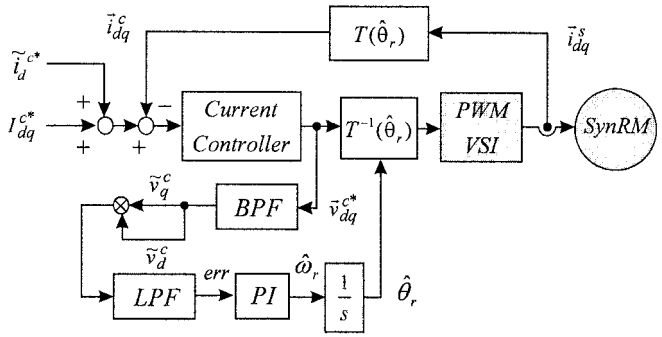

Fig. 3. Rotor angle estimation by high-frequency current injection.

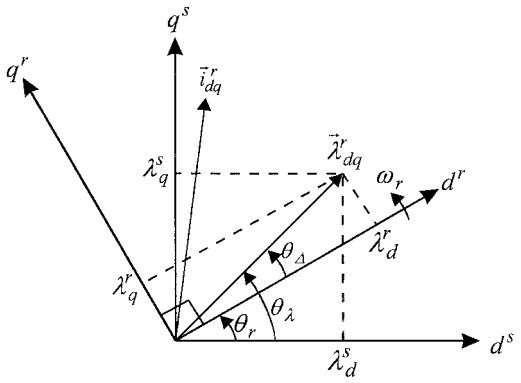

Fig. 4. Current vector and stator flux vector.

follows:

$$\begin{aligned}\text{err} &= \text{LPF}(\tilde{v}^c_q \cdot \tilde{v}^c_d) \\ &\approx \frac{1}{4}L_d(L_d - L_q)\ \sin 2\Delta\theta_r \omega_h^2 I_h^2 \\ &\approx \frac{1}{2}L_d(L_d - L_q)\omega_h^2 I_h^2 \Delta\theta_r \\ &= Z_{\text{err}}\Delta\theta_r \end{aligned} \tag{13}$$

where

$$\begin{aligned}\Delta\theta_r &= \theta_r - \hat{\theta}_r \\ Z_{\text{err}} &\equiv \frac{1}{2}L_d(L_d - L_q)\omega_h^2 I_h^2\end{aligned}$$

and LPF is a low-pass filter.

The error is in the form of a linear angle error, such as (13). This error can be driven away using the scheme shown in Fig. 3. Then, the frequency-response function relating the estimated and actual rotor angles is as follows:

$$\frac{\hat{\theta}_r(s)}{\theta_r(s)} = \frac{K_1 s + K_2}{s^2 + K_1 s + K_2} \tag{14}$$

where the controller $G(s) = (1/s)(K_P + (K_I/s))$ and

$$\begin{aligned}K_1 &= Z_{\text{err}}K_P \\ K_2 &= Z_{\text{err}}K_I.\end{aligned}$$

As can be seen from (14), the transfer function has the form of second-order low-pass filter, the estimated rotor angle converges to the real rotor angle in a low-speed region, and the estimation of rotor position is independent of load condition. Despite the fact that the d and q inductance parameters are used in (13), the detuned parameters do not influence the accuracy of the estimation, since they are just gains of the estimator.

B. High-Speed Region—Stator Flux Estimation

As the operating frequency increases, the controllable voltage margin decreases because of the voltage drop by the injected high-frequency current signal. Moreover, the injected current causes additional losses and noise. Therefore, it is effective for estimating the rotor position based on the stator flux from the voltage information in a high-speed region, since there is a sufficient magnitude of voltage information.

Fig. 4 shows the relation of the stator flux vector and current vector. The stator flux in the stationary reference frame d^s, q^s can be estimated by integrating the stator voltage as

$$\vec{\lambda}^s_{dq} = \int (\vec{v}^s_{dq} - r_s \vec{i}^s_{dq})\, dt. \tag{15}$$

The angle of stator flux $\hat{\theta}_\lambda$ can be calculated as

$$\hat{\theta}_\lambda = \tan^{-1}(\lambda^s_q/\lambda^s_d). \tag{16}$$

There is an angle difference θ_Δ between the stator flux vector and the rotor angle. Then, the rotor angle is estimated from the angle of stator flux and motor currents as

$$\hat{\theta}_r = \hat{\theta}_\lambda - \tan^{-1}\left(\frac{L_q i^c_q}{L_d i^c_d}\right). \tag{17}$$

In the stator flux estimation, the parameter of the stator resistance is included and the detuned value may deteriorate the rotor-position estimation. However, the voltage drop due to the resistance is relatively small in the high-speed region, and its value can be easily set by off-line tuning.

Fig. 5 shows the overall block diagram of proposed sensorless controller. High-frequency currents are injected into the d, q reference currents, and the rotor angle is estimated in a low-speed region. In a high-speed region, the rotor angle is estimated from the stator flux and currents without injecting high-frequency currents. Position and speed control are performed based on the estimated position and speed. There can be an error between the estimated angles of two different methods, and this makes chattering or the stability problem in transition. To achieve a seamless transition of two estimation methods, the parameter α is introduced. $\hat{\theta}_{r\,\text{inj}}$ is the estimated position by high-frequency current injection, and $\hat{\theta}_{r\,\text{flux}}$ is that by stator flux estimation and is unity in a low-speed region and zero in a high-speed region, and it has a finite slope in the transition period. Then, the estimated rotor position can be represented as

$$\hat{\theta}_r = \alpha\hat{\theta}_{r\,\text{inj}} + (1-\alpha)\hat{\theta}_{r\,\text{flux}}. \tag{18}$$

The estimation of rotor speed can be made by differentiating the estimated rotor position. However, the direct differentiation causes the noise problem and essentially requires the low-pass filtering which suffers from the phase delay. Therefore, the

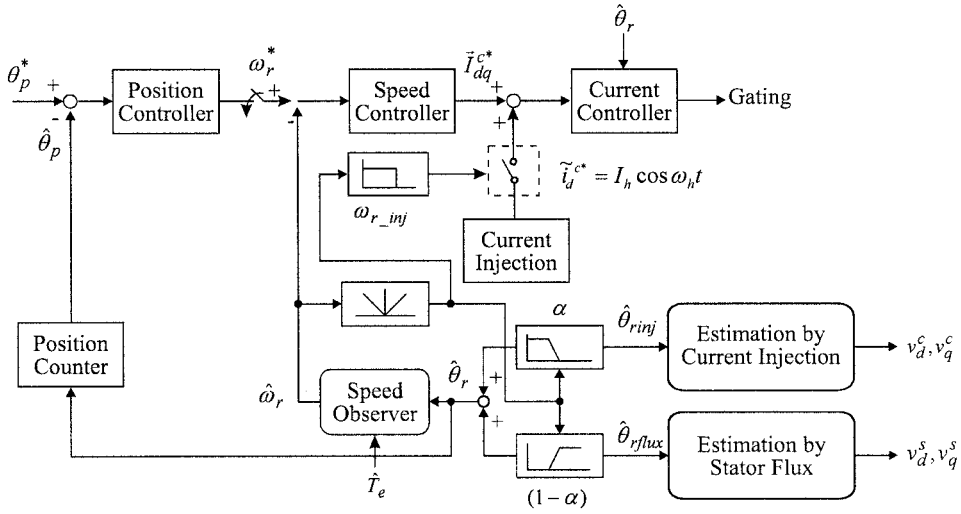

Fig. 5. Block diagram of the proposed sensorless drive.

TABLE I
PARAMETERS OF SYNRM

Rated power	3.75 kW
Rated speed	1800 r/min
Rated torque	19.8 N·m
r_s	0.238 Ω
L_d	43.0 mH
L_q	3.5 mH

speed observer using the estimated position and torque has been introduced to estimate the rotor speed as shown in Fig. 5 [14].

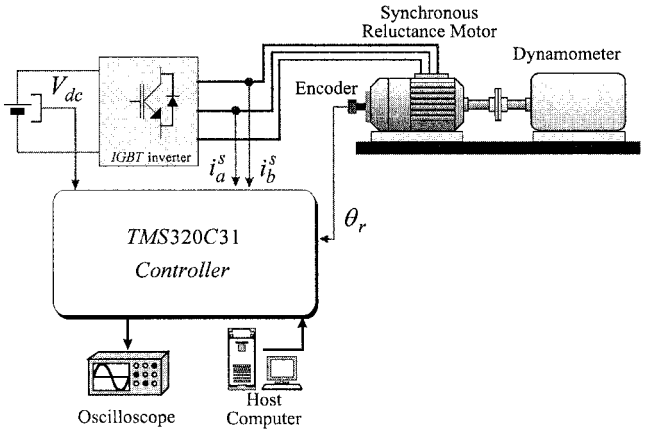

Fig. 6. Block diagram of experimental setup.

III. EXPERIMENTAL RESULTS

To validate the performance of the proposed method, an experimental setup with a 3.75-kW axially laminated SynRM has been built. The stator has been derived from that of a conventional induction motor, and the rotor has been designed and built. The parameters of the machine are shown in Table I.

The experiment with the proposed controller was conducted using a TMS320C31 digital signal processor (DSP). The overall execution time of the proposed scheme, including the rotor angle estimation, d–q transform, high-frequency current injection and/or stator flux estimation, current control, and space-vector pulsewidth modulation (PWM) is about 70 μs with a 40-MHz clock. The configuration of the experimental system is shown in Fig. 6. The experimental system contains an insulated gate bipolar transistor (IGBT) PWM inverter, a SynRM, and a DSP control board. A personal computer is used to command the speed or position reference.

The switching devices in the inverter are IGBT's with 5-kHz switching frequency. The sampling time of the current controller is 100 μs and that of the speed controller is 1 ms. The injected frequency ω_h for estimation is 200 Hz, and its magnitude I_h is 1.5 A, which is 0.06 p.u. of rated current. The influence of injected currents on the overall performance is relatively small because its frequency is sufficiently high and its magnitude is small. The high-frequency current is injected in the speed range from −125 to 125 r/min. The transition of estimation methods occurs between ±80–±90 r/min by combining the estimated positions of two methods to ensure the seamless transition.

The speed reversal performance at very low speed is shown in Fig. 7. The speed reference is changed from 20 to −20 r/min with 0.5-p.u. load condition. The speed control is stable at transient and steady state. The existence of a period of zero speed is due to the characteristics of load, which is an eddy-current-type dynamometer which provides only friction-type torque. It can be seen that the estimated position coincides well with the actual position in the low-speed region. Fig. 8 illustrates the responses of the speed reversal with high speed; the speed reference is changed from 1000 to −1000 r/min with no-load condition. In this condition, there is a transition of two estimation methods

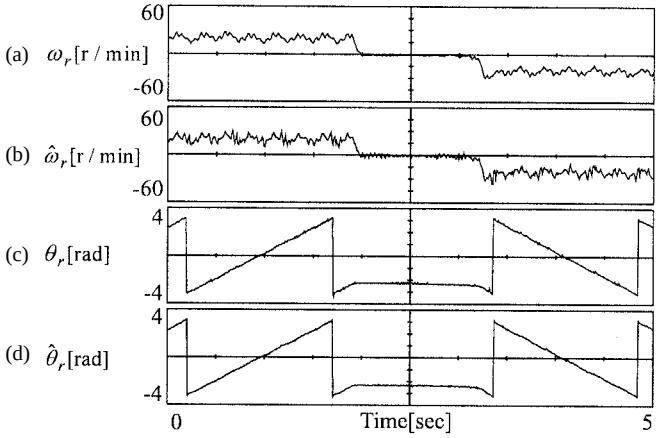

Fig. 7. Speed reversal of the proposed method (± 20 r/min, 0.5-p.u. load). (a) Actual speed. (b) Estimated speed. (c) Actual angle. (d) Estimated angle.

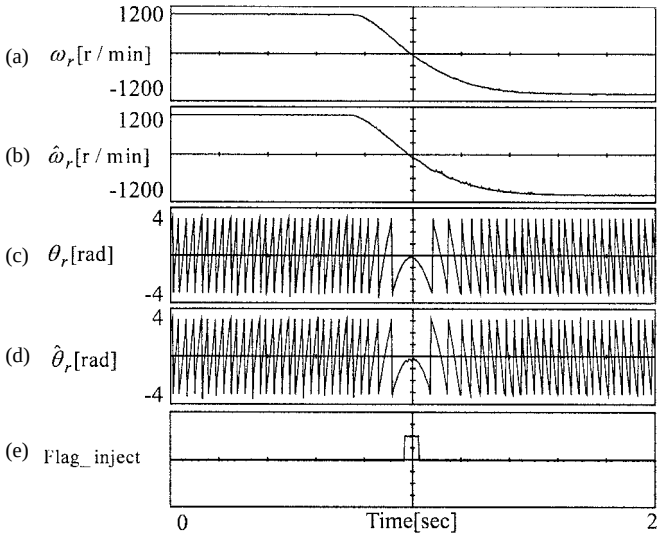

Fig. 8. Speed reversal of the proposed method (± 1000 r/min, no load) (a) actual speed (b) estimated speed (c) actual angle (d) estimated angle (e) flag of high frequency current injection.

according to the operating speed. In Fig. 8(e), the period of high-frequency current injection is displayed. It can be seen that the proposed estimation scheme operates well with seamless transition between two methods. Fig. 9 is the same condition as the case of Fig. 8, except the load is 1 p.u. Even with the full-load condition, the proposed estimator operates as shown in Figs. 7–9. The proposed sensorless scheme reveals the characteristics at expected operating conditions.

With the tracking ability in the overall speed region including zero speed, the closed-loop position control is tested. Figs. 10 and 11 show the performance of the position control. The step position reference is $\pm(0.5 \times \pi)$ rad (mechanical angle) with full-load condition in Fig. 10 and $\pm(20 \times \pi)$ rad (mechanical angle) with 0.5-p.u. load in Fig. 11. The transition between two estimating methods occurs in Fig. 11, and only the current injection scheme operates in Fig. 10 because of the speed range. The estimated and real position and speed coincide well in each figure, and the position error, which is calculated from the position reference, and the real position

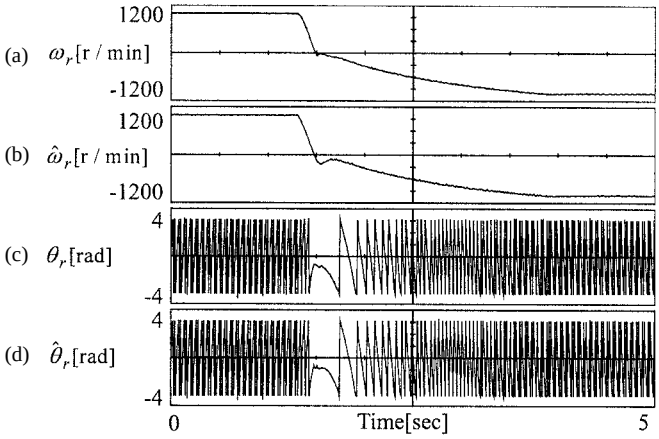

Fig. 9. Speed reversal of proposed method (± 1000 r/min, full load). (a) Actual speed. (b) Estimated speed. (c) Actual angle. (d) Estimated angle.

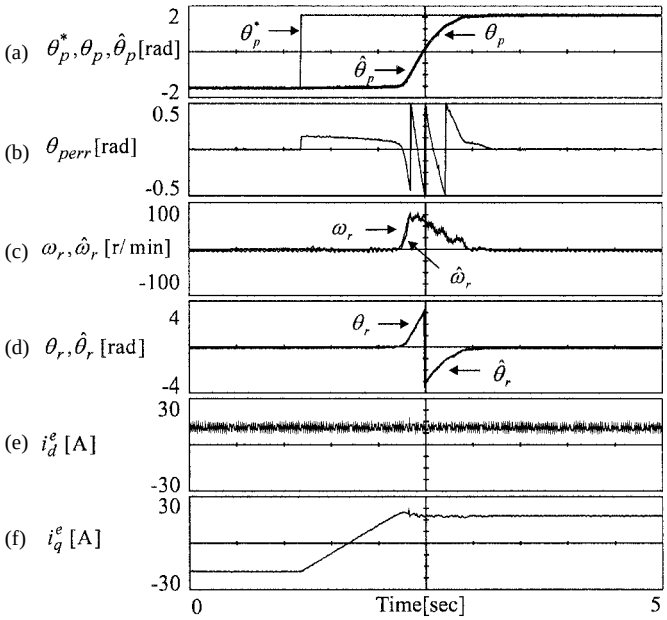

Fig. 10. Position control characteristics ($-\pi/2 \rightarrow \pi/2$ rad (mechanical angle), full load). (a) Reference, real position, and estimated position. (b) Position error. (c) Actual and estimated speed. (d) Actual and estimated angle. (e) d-axis current. (f) q-axis current.

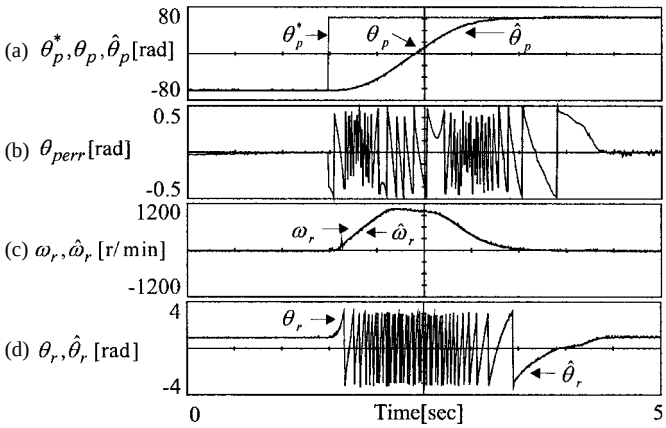

Fig. 11. Position control characteristics ($-20\pi \rightarrow 20\pi$ rad (mechanical angle), 0.5-p.u load). (a) Reference, real position, and estimated position. (b) Position error. (c) Actual and estimated speed. (d) Actual and estimated angle.

converge to zero. From the d, q currents of Fig. 10(e) and (f), it can be seen that the closed-loop position control is possible even with full-load condition.

IV. Conclusions

A position sensorless control scheme of a SynRM combining the high-frequency current injection method in a low-speed region and the flux estimation method based on the stator voltages in a high-speed region has been presented. The rotor has inherent saliency, and its angle is estimated from d-axis stator current injection and the appropriate signal demodulation in a low-speed region. The stator flux and rotor angle are estimated from the voltage information in a high-speed region. Experimental results of speed and position control have been demonstrated with a 3.75-kW axially laminated SynRM. The results reveal a robust and dynamic estimation performance of the rotor angle, independent of the operating condition.

References

[1] T. Matsuo and T. A. Lipo, "Field oriented control of synchronous reluctance machine," in *Proc. IEEE PESC'93*, 1993, pp. 425–431.
[2] R. E. Betz, R. Lagerquist, M. Jovanovic, T. J. E. Miller, and R. H. Middleton, "Control of synchronous reluctance machines," *IEEE Trans. Ind. Applicat.*, vol. 29, pp. 1110–1121, Nov./Dec. 1993.
[3] L. Xu and J. Yao, "A compensated vector control scheme of a synchronous reluctance motor including saturation and iron loss," *IEEE Trans. Ind. Applicat.*, vol. 28, pp. 1330–1338, Nov./Dec. 1992.
[4] S. Bolognani, "A torque angle calculator for sensorless reluctance motor drives," in *Proc. 1991 European Power Electronics Conf.*, vol. 4, pp. 13–17.
[5] M. S. Arefeen and M. Ehsani, "Sensorless position measurement in synchronous reluctance motor," *IEEE Trans. Power Electron.*, vol. 9, pp. 624–630, Nov. 1994.
[6] R. Lagerquist, I. Boldea, and T. J. Miller, "Sensorless control of the synchronous reluctance motor," *IEEE Trans. Ind. Applicat.*, vol. 30, pp. 673–682, May/June 1994.
[7] L. Kreindler, A. Testa, and T. A. Lipo, "Position sensorless synchronous reluctance motor drive using the stator phase voltage third harmonic," in *Conf. Rec. IEEE-IAS Annu. Meeting*, 1993, pp. 679–686.
[8] T. Matsuo and T. A. Lipo, "Rotor position detection scheme for synchronous reluctance motor based on current measurement," *IEEE Trans. Ind. Applicat.*, vol. 31, pp. 860–868, July/Aug. 1995.
[9] M. Schroedl and P. Weinmeier, "Sensorless control of reluctance machines at arbitrary operating conditions including standstill," *IEEE Trans. Power Electron.*, vol. 9, pp. 225–231, Mar. 1994.
[10] E. Cerruto, A. Consoli, A. Raciti, and A. Testa, "Slip gain tuning in indirect field oriented control drives," *Elect. Mach. Power Syst.*, vol. 23, no. 1, pp. 63–80, 1995.
[11] S. I. Yong, J. W. Choi, and S. K. Sul, "Sensorless vector control of induction machine using high frequency current injection," in *Conf. Rec. IEEE-IAS Annu. Meeting*, 1994, pp. 503–508.
[12] J. I. Ha and S. K. Sul, "Sensorless field orientation of an induction machine by high frequency signal injection," in *Conf. Rec. IEEE-IAS Annu. Meeting*, 1997, pp. 426–432.
[13] P. L. Jansen and R. D. Lorenz, "Transducerless position and velocity estimation in induction and salient AC machines," *IEEE Trans. Ind. Applicat.*, vol. 31, pp. 240–247, Mar./Apr. 1995.
[14] G. F. Franklin, J. D. Powel, and A. Emami-Naeini, *Feedback Control of Dynamic Systems*. Reading, MA: Addison-Wesley, 1991, pp. 397–411.

Jung-Ik Ha (S'97), for a photograph and biography, see p. 51 of the January/February 1999 issue of this Transactions.

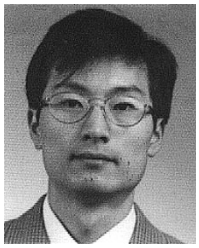

Seog-Joo Kang (S'92–M'98) received the B.S., M.S., and Ph.D. degrees in electrical engineering from Seoul National University, Seoul, Korea, in 1991, 1993, and 1998, respectively.

He is currently with the Building Systems Research Laboratory, LG Industrial Systems Company, Ltd., Incheon, Korea. His research interests are electrical machines, elevator control, and high-performance ac drives.

Seung-Ki Sul (S'78–M'80–SM'98), for a photograph and biography, see p. 51 of the January/February 1999 issue of this Transactions.